

Detection of Deep-Levels in Doped Silicon Nanowires Using Low-Frequency Noise Spectroscopy

Deepak Sharma, Abhishek Motayed, Sergiy Krylyuk, Qiliang Li, *Member, IEEE*, and Albert V. Davydov

Abstract—We report detailed characterization of electrically-active deep-levels in doped Si nanowires (SiNWs) grown using catalyst-assisted vapor-liquid-solid (VLS) technique. Temperature-dependent low-frequency noise (LFN) spectroscopy was used to reveal the presence of generation-recombination related Lorentzian-type peaks along with $1/f$ -type noise in these NWs. In Ni-catalyzed SiNWs, the correlated LFN spectroscopy detected electrically active deep-levels with ionization energies of 0.42 eV for the n-type and 0.22 eV for the p-type SiNWs, respectively. In Au-catalyzed n- and p-type SiNWs, the energies of the deep-levels were estimated to be 0.44 and 0.38 eV, respectively. These values are in good agreement with the known ionization energies of deep-levels introduced by Ni and Au in Si. Associated trap concentrations and hole and electron capture cross sections were also estimated. This paper clearly indicated the presence of electrically active deep-levels associated with unintentional incorporation of catalyst atoms in the VLS-grown SiNWs.

Index Terms—Deep-levels, field-effect transistor (FET), generation-recombination (G-R) noise, low-frequency noise (LFN), silicon nanowire (SiNW).

I. INTRODUCTION

SEMICONDUCTOR nanostructures are revolutionizing the field of electronics through realization of high-performance devices and development of new understanding of transport mechanisms in such confined geometries [1]–[7]. Due to the small number of charge carriers present in such nanostructures, understanding the role of defects, whether present in the bulk or at the interface, in charge carrier transport becomes increasingly important [8]–[10].

Manuscript received July 1, 2013; accepted October 2, 2013. Date of publication October 21, 2013; date of current version November 20, 2013. This work was supported by the National Science Foundation under Grant ECCS-0112802 to the University of Maryland, College Park, MA, USA. The review of this paper was arranged by Editor Z. Celik-Butler.

D. Sharma is with the Department of Electrical and Computer Engineering, George Mason University, Fairfax, VA 22030 USA, and also with the National Institute of Standards and Technology, Material Measurement Laboratory, Gaithersburg, MD 20899 USA (e-mail: dsharma6@gmu.edu).

A. Motayed and S. Krylyuk are with IREAP, University of Maryland, College Park, MD 20742 USA, and also with the National Institute of Standards and Technology, Material Measurement Laboratory, Gaithersburg, MD 20899 USA (e-mail: abhishek.motayed@nist.gov; sergiy.krylyuk@nist.gov).

Q. Li is with the Department of Electrical and Computer Engineering, George Mason University, Fairfax, VA 22030 USA (e-mail: qlif@gmu.edu).

A. V. Davydov is with the National Institute of Standards and Technology, Material Measurement Laboratory, Gaithersburg, MD 20899 USA (e-mail: albert.davydov@nist.gov).

Color versions of one or more of the figures in this paper are available online at <http://ieeexplore.ieee.org>.

Digital Object Identifier 10.1109/TED.2013.2285154

It is well-known that the electrically active defects in semiconductors often act as unintended generation-recombination (G-R) centers, adversely affecting the carrier lifetimes and device performance [11]. Despite tremendous advances made in the fabrication techniques of such nanostructures, both top-down [12] and bottom-up [13] approaches, there is still a vital need for measurement techniques for characterization of electrically active defects in nanoscale devices. This stems from the fact that the conventional methods to study deep-levels such as deep-level transient spectroscopy (DLTS) and photoinduced current transient spectroscopy (PICTS) become impractical for nanoscale devices [14]. Recently, Sato *et al.* [15] demonstrated DLTS and PICTS measurements on Si nanowire (SiNW) arrays using top-contact geometry for contacting large number of NWs. Applying those measurements on single NW devices is difficult.

In [16], we have shown the use of low-frequency noise (LFN) spectroscopy to characterize G-R centers in SiNWs grown using catalyst-assisted chemical vapor deposition (CVD). In this paper, we implemented LFN spectroscopy using technique, which utilizes cross-correlation method to reduce instrument noise [17]. This method was applied to probe deep-levels in p- and n-type SiNWs grown by the vapor-liquid-solid (VLS) mechanism using Au and Ni catalysts. Noise measurements were performed in 160- to 320-K temperature range. The power spectrum density (PSD) spectra showed clear Lorentzian behavior in all NW field-effect transistors (FETs) due to the G-R processes. Temperature-dependent noise analysis strongly indicated that the traps responsible for the G-R noise are due to the deep-levels introduced by Ni and Au atoms, which diffused unintentionally into the Si lattice during the VLS growth.

II. EXPERIMENTAL DETAILS

A. NW Growth and Doping

The VLS growth of Au- and Ni-catalyzed SiNWs was carried out in a custom-built hot wall CVD system at a reactor pressure of 80 kPa (600 Torr) using 30 sccm of silicon tetrachloride (SiCl_4) and 200 sccm of hydrogen further diluted with nitrogen to a total flow rate of 1000 sccm. For gold-catalyzed NWs, 100-nm Au nanoparticles were cast on poly-L-lysine-functionalized Si (111) substrates. The NWs were then grown at 900 °C for 10 min, resulting in ≈ 25 - μm -long SiNWs with an average diameter of 130 nm.

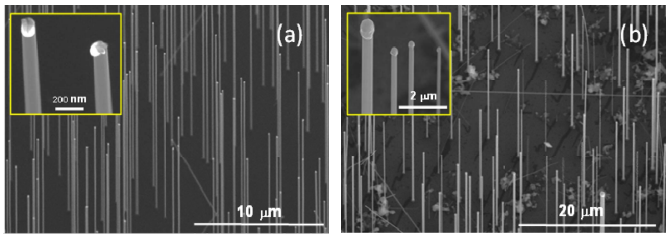


Fig. 1. (a) and (b) Bird's-eye view SEM images of Au- and Ni-catalyzed Si NWs grown at 900 °C and 1000 °C, respectively. Insets show magnified top sections of the NWs capped with the metal catalyst tips.

To minimize postgrowth migration of the Au catalyst from the tips of SiNWs, the samples were rapidly cooled to ≈ 550 °C by transferring them to the cold zone of the reactor. The Ni-catalyzed SiNWs were grown at 1000 °C for 5 min. The Ni islands, which served as nucleation sites for the NW growth, were preformed on Si (111) substrate by thermal dewetting of e-beam deposited 2-nm-thick Ni film. Diameters of these NWs varied between 100 and 600 nm and the growth rate was 10 $\mu\text{m}/\text{min}$. The n- and p-type doping was achieved by adding PH_3 (100 ppm in N_2) and BCl_3 (2% in N_2), respectively, to the gas mixture with P(B)/Si ratio of 1.3×10^{-6} (3.3×10^{-4}).

Representative scanning electron microscope (SEM) images of vertical array of Au- and Ni-catalyzed SiNWs are shown in Fig. 1(a) and (b), respectively. The hexagonal-prism-shaped NWs grew normal to the Si (111) substrate along the $\langle 111 \rangle$ direction and were bound by six $\{1\ 1\ 2\}$ sidewall facets as confirmed by transmission electron microscopy (TEM) (data not shown). The TEM also revealed that the NWs were free from extended structural defects.

B. Device Fabrication

A suspension of NWs was formed by sonicating the growth substrate in isopropanol. FET devices were fabricated by randomly dispersing the SiNWs on a heavily doped p-type Si-substrate with 1- μm -thick SiO_2 layer deposited using plasma-enhanced chemical vapor deposition (PECVD). The dispersed NW samples were cleaned in O_2/Ar (1:5) plasma and conformally coated with 50 nm of PECVD SiO_2 layer. The top oxide layer that passivates the NW surface was found to be crucial for enabling reproducible device measurements. Photolithography was done on the oxide coated NWs to define the source and drain contact openings. The oxide on the openings was etched using reactive ion etching with $\text{CF}_4/\text{CHF}_3/\text{O}_2$ (50/25/5 sccm) gas mixture. The source/drain metallization stack Ti (70 nm)/Al (70 nm)/Ti (30 nm)/Au (30 nm) was deposited using an e-beam system and annealed in a rapid thermal processing system at 550 °C for 30 s with 6000-sccm flow of Ar. The back-gate contact was formed by e-beam depositing 200-nm-thick Al layer onto the back side of the Si substrate.

Four sets of FETs were fabricated: 1) n-type SiNWs grown using Ni catalysts; 2) n-type SiNWs grown using Au catalysts; 3) p-type SiNWs grown using Ni catalysts; and 4) p-type SiNWs grown using Au catalysts.

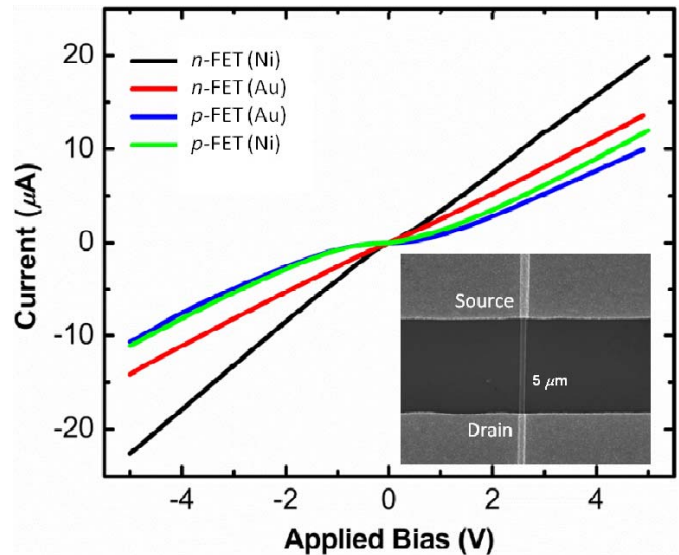


Fig. 2. Room-temperature I - V curves of four different types of SiNW FETs. The I - V curves were taken at zero gate-source voltage (V_{GS}). The inset is a plan-view SEM image of representative NWFET with channel length of 5 μm and NW diameter 140 nm.

C. Parametric Measurements and LFN Spectroscopy

The temperature-dependent parametric measurement was done in an open-cycle cryogenic probe station using Agilent B1500A semiconductor parameter analyzer.¹ The noise of the current amplifiers often sets the lower limit of detection in conventional LFN measurements. Our LFN measurement setup is based on the work done by Sampietro *et al.* [17], who demonstrated subtraction of the instrument noise using cross correlation technique. Two independent current amplifiers (SR570 from Stanford Research Systems) provided the source-drain bias and the gate bias is provided by an independent battery. The temperature-dependent measurements were performed from 160 to 320 K, starting from the lowest temperature. The LFN measurements were conducted between 1 and 1000 Hz with frequency resolution of 0.25 Hz. The dynamic signal analyzer had maximum of 4096 fast Fourier transform points, which resulted in 1600 frequency resolution lines for a given time record. Thus, in order to obtain 0.25-Hz resolution, the measurement span of 1000 Hz was broken down into three smaller spans of 400 Hz. Measurement in each 400-Hz span was root-mean-square averaged, which resulted in 4 min of total data acquisition time for the entire 1000-Hz span. The increased frequency resolution was essential for determining the G-R peaks appearing on the $1/f$ spectra.

III. RESULTS AND DISCUSSION

A. Device Characterization

The current-voltage (I - V) curves of different NW FETs are shown in Fig. 2. Inset in Fig. 2 shows an SEM image

¹Certain commercial equipment, instruments, or materials are identified in this paper to foster understanding. Such identification does not imply recommendation or endorsement by the National Institute of Standards and Technology nor does it imply that the materials or equipment identified are necessarily the best available for the purpose.

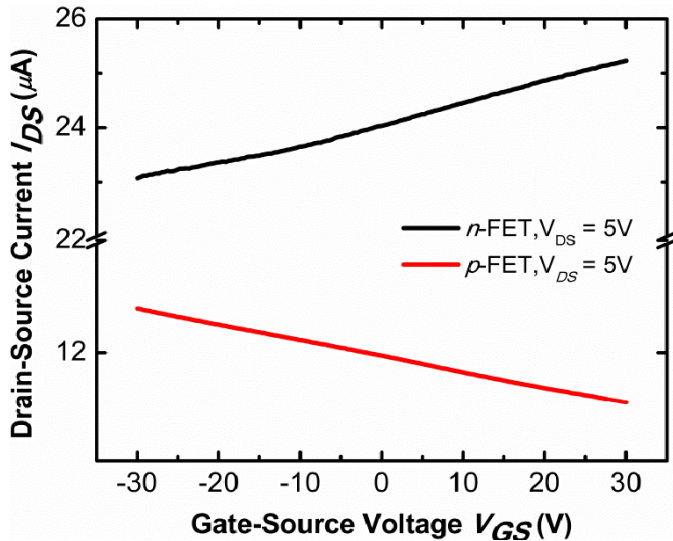


Fig. 3. I_{DS} versus V_{GS} plot of n -type and p -type Ni-catalyzed SiNW FETs.

of a complete SiNW FET. It is worth noting that the n -type NWs always had linear I - V characteristics, whereas p -type devices showed nonlinearity in ± 0.3 V range. This most likely resulted from the fact that the doping levels in n -type NWs were slightly higher than the p -type NWs.

The drain-source current (I_{DS}) as a function of gate-source voltage (V_{GS}) for n - and p -type Ni-catalyzed SiNWs is shown in Fig. 3. The slopes of the plots are consistent with the dopant types in both types of NWs, i.e., reduction in channel current with decreasing gate voltage for n -type NWs and vice versa for p -type NWs. Similar trends were observed for Au-catalyzed wires (not shown). The calculated field-effect carrier mobilities at 300 K for pFET (Ni) and nFET (Ni) are in the range of 25 – 40 $\text{cm}^2 \text{V}^{-1} \text{s}^{-1}$ and 5 – 15 $\text{cm}^2 \text{V}^{-1} \text{s}^{-1}$, respectively. The mobility values are consistent with the calculated dopant density of 1 – $5 \times 10^{18} \text{cm}^{-3}$ for p -type and 1 – $5 \times 10^{19} \text{cm}^{-3}$ for n -type NWs for both Ni- and Au-catalyzed NWs.

B. Temperature-Dependent Resistivity

Fig. 4 shows the source-drain resistance for SiNW FETs as a function of measurement temperature. Arrhenius plot shows semiconducting behavior in all NWs. Using the relationship $\ln(R) = \ln(R_0) + E_a/(2k_B T)$ (where R_0 is the intercept, E_a is the activation energy, k_B is the Boltzmann's constant, and T is the absolute temperature), we calculated the activation energy for conduction in all four types of SiNWs. For Au-catalyzed NWs, activation energies obtained for p - and n -FETs were 0.06 and 0.04 eV, respectively. For Ni-catalyzed NWs, the estimated activation energies were 0.09 eV for n -type and 0.06 eV for p -type FETs [18]. A close match with expected activation energy of shallow-dopant related conduction is only found in the case of Au-catalyzed p -type NWs. Higher values obtained for the rest of the NWs could have been influenced by contribution from the contact resistances, as these measurements were conducted using two-terminal structures. Nevertheless, these results point to the fact that the dc conduction in these NWs is dominated by shallow dopants.

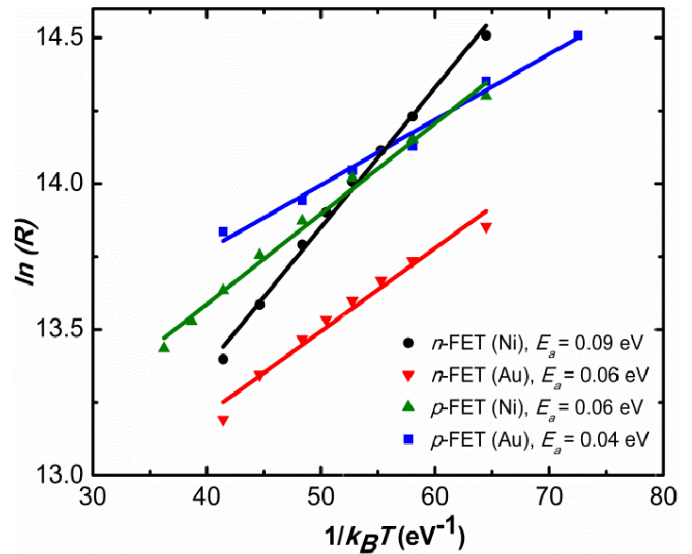


Fig. 4. Arrhenius plot of the drain-source resistance in the linear region of the four different SiNW FETs shown in Fig. 2. For all four types of NWs, good fit to the activation energy model is evident.

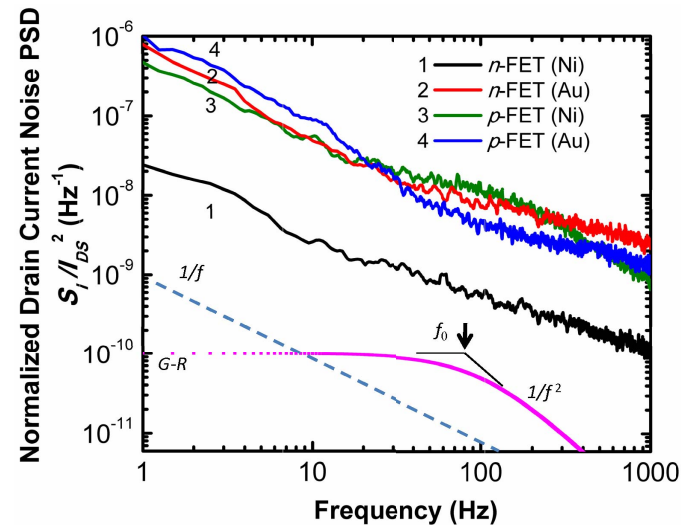


Fig. 5. Normalized PSD of the drain-current noise of four types of SiNW FETs (same as shown in Fig. 4) at 290 K. The $1/f$ trend is shown by the blue dotted line. The ideal single-time constant Lorentzian-type PSD is shown by the dotted magenta line, where the black arrow indicates the characteristic rollover frequency.

C. LFN Spectroscopy

The normalized drain-current noise PSD is defined as $S_I(f)^2/I_{DS}^2 = \langle i_{ds}(f)^2 \rangle / \Delta f I_{DS}^2$, where $\langle i_{ds}(f)^2 \rangle$ is the mean-square value of the current fluctuations with a particular frequency, Δf is the effective measurement bandwidth for the discrete frequency point, and I_{DS} is the dc value of the drain current. Normalized PSD for four different SiNW FETs are shown in Fig. 5. For reference, the $1/f$ trend line is also shown, and deviation from the $1/f$ behavior is clearly seen in all the curves. The curves in Fig. 5 are the representatives of ~ 10 NW devices of each type.

Significantly, lower level of noise has been systematically observed for Ni-catalyzed n -type NWs (curve 1 in Fig. 5).

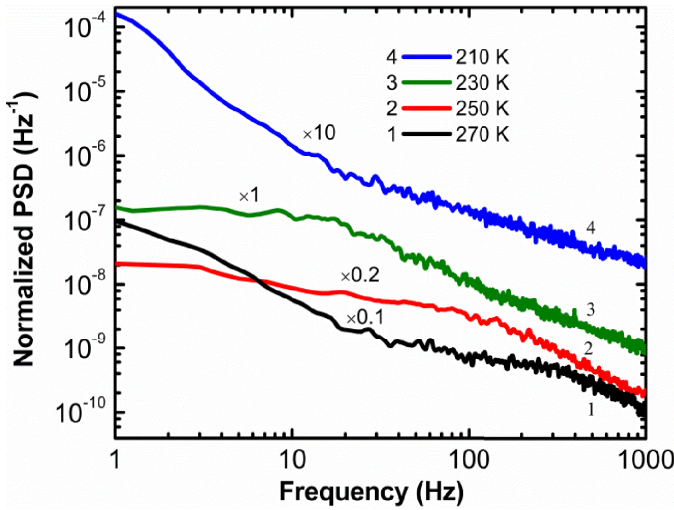


Fig. 6. Normalized PSD of the drain current noise of Ni-catalyzed p-type wires taken at different temperatures. The shift of the characteristics corner frequency of the Lorentzian-type PSD with decreasing temperature can be clearly seen. The curves are scaled for better visualization, with the scaling factor indicated above each curve.

Typically for a device that exhibits $1/f$ -type noise, irrespective of the cause of the noise, the normalized noise PSD can be described by the relationship $S_I/I_{DS}^2 = \alpha_H/Nf^\beta$, where α_H is the Hooge's constant, N is the total number of carriers, and the exponential factor β is ideally 1 [19]. The Hooge's constant is a generally accepted indicator of the quality of materials in terms of noise, i.e., the lower the Hooge's constant, the higher the material quality. We estimated the Hooge's constant for all the NWs at 1 Hz, where the PSD is nearly $1/f$. For all the NWs, except Au-catalyzed n-type NWs, the estimated Hooge's constant was in the range of 0.07–0.04, with the lowest values estimated for Ni-catalyzed n-type NWs. This is consistent with the lower PSD values observed in these NWs. The estimated Hooge's constant value for Au-catalyzed n-type NWs was in the range of 0.2–0.6. Our previously reported value on p-type Au-catalyzed wires was in the same range [16].

At room-temperature, the drain-current noise PSD in SiNWs clearly showed a Lorentzian-behavior

$$S_I \propto \tau / (1 + \omega^2 \tau^2) \quad (1)$$

where τ is the relaxation time of the G-R process, and ω is related to the measurement frequency ($\omega = 2\pi f$) [20]. The noise PSD due to a pure single time-constant G-R process is constant till the cutoff frequency f_0 ($\tau = 1/f_0$), above which it rolls off as $1/f^2$ (the theoretical G-R PSD characteristic is shown in Fig. 5 by the dotted magenta line). It is well-known that the Lorentzian-type PSD is due to the fluctuations of the charge states of the Shockley–Reed–Hall G-R centers present in bulk material [11]. There could be other mechanisms in NWs that generate LFN such as surface noise, contact noise, shallow dopant fluctuation noise, and Auger G-R noise. Band-bending at the surface provides continually varying time-constants associated with the G-R centers resulting in a $1/f$ -type noise distribution [21]. Contact noise either due to thermal activation or tunneling would yield a $1/f$ -type LFN as

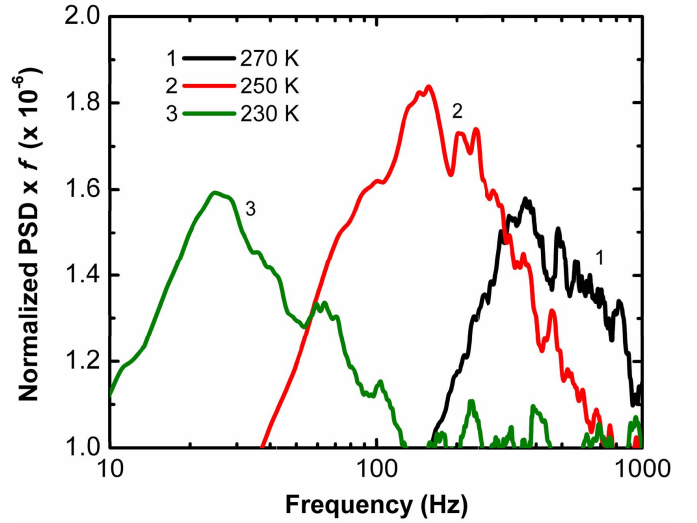


Fig. 7. Semilog plot of PSD $\times f$ for Ni-catalyzed p-type SiNW at different temperatures. The Lorentzian shape of the peak and its shift with temperature can be clearly seen. Normalized PSD is taken from Fig. 6.

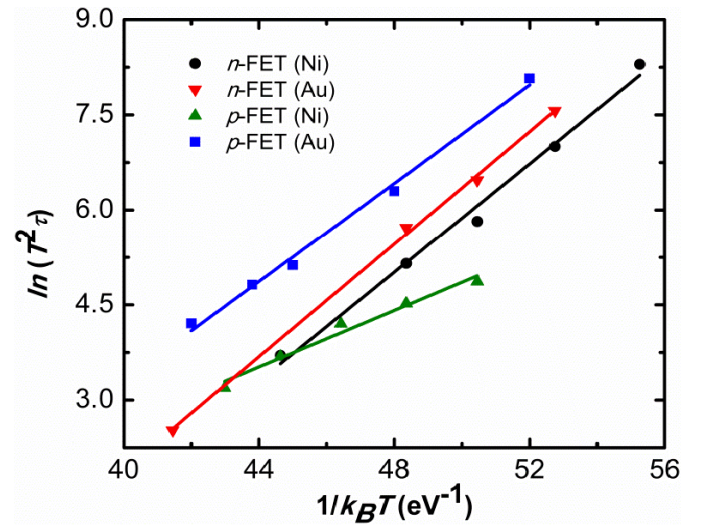


Fig. 8. Arrhenius plot of the $\ln(T^2\tau)$ versus $1/k_B T$ of different types SiNW FETs.

well [22]. The shallow dopant-related capture and emission events are rare at the measurement temperature range. Although trap-assisted Auger G-R process becomes significant at high dopant concentrations, the time-constants associated with such processes will be in the range of 10^{-5} s [23], whereas the time-constants observed here are in range of 10^{-3} s. Thus, it is most likely that the Lorentzian-type PSD seen in these NWs is associated with single time-constant G-R processes happening at the discrete states within the bandgap inside the NW.

However, often deviation from the single-time constant curve is observed, especially at low frequencies, where surface-related $1/f$ noise dominates [24]. In [16], LFN in Au-catalyzed boron-doped NWs was presented, which exhibited the ideal single-time constant behavior. The characteristic time-constant τ in (1) associated with fluctuations of the G-R

TABLE I
ESTIMATED ENERGIES, CAPTURE CROSS SECTIONS, AND CONCENTRATIONS OF TRAPS IN SiNWs

Catalyst	Doping	Calculated Trap Energy (eV)	Calculated Capture Cross-sections (cm ²)		Estimated Trap Concentration(cm ⁻³)
			Electron	Hole	
Ni	<i>n</i> -type	0.42	6.1×10^{-15}	5.3×10^{-15}	1.0×10^{12}
Ni	<i>p</i> -type	0.22	5.7×10^{-19}	5.0×10^{-19}	1.0×10^{16}
Au	<i>n</i> -type	0.44	8.4×10^{-15}	7.3×10^{-15}	1.8×10^{12}
*Au	<i>p</i> -type	0.38	9.5×10^{-17}	1.4×10^{-16}	2.0×10^{12}

* - data for *p*FET(Au) are from our previous paper [16], which are in good agreement with the DLTS and PICTS derived data in [15].

TABLE II
ENERGY LEVELS IN BULK SI INTRODUCED BY Ni AND Au [32]

Metal	Type	Trap Energy (eV)
Ni	Acceptor	$E_c - 0.41$
	Donor	$E_v + 0.17$
Au	Acceptor	$E_c - 0.55$
	Donor	$E_v + 0.34$

process is given by [25]

$$\tau = 1/(c_n n + e_n + c_p p + e_p) \quad (2)$$

where c_n , c_p are the electron and hole capture coefficients, e_n , e_p are the electron and hole emission coefficients, and n , p are the equilibrium electron and hole concentrations, respectively. Temperature-dependence of τ comes from the temperature dependence of carrier concentration, and from (2), it is easy to see that the decrease in carrier concentrations with decreasing temperature will result in an increase in the time constant, i.e., in a decrease of the rollover frequency f_0 . This is exemplified in Fig. 6, which shows normalized PSD of the drain-current noise for *p*-type Ni-catalyzed SiNW FETs taken at different temperatures. As expected, we can see the decrease in the rollover frequency as the temperature is decreased. For determination of the characteristic (rollover) frequency, it is very convenient to plot the product of normalized PSD $\times f$ in a linear scale as a function of the frequency in a log scale as shown in Fig. 7. In this representation, the PSD $\times f$ product appears as a Lorentzian-shaped symmetric peak centered at f_0 . The characteristic frequency f_0 (and hence the time-constant τ) for each temperature can be determined by fitting the corresponding curve to a Lorentzian function. Using this method, we found temperature dependences of the time-constants for all types of SiNWs studied here. The time-constant τ associated with current fluctuations due to a G-R process can be related to the trap energy-level and capture

cross section by the relationships [26], [27]

$$\ln(T^2 \tau) \approx \left(\frac{\Delta E}{k_B T} \right) - \ln \left[\left(\frac{4k_B^2 \sigma_n}{gh^3} \right) \left(6\pi^3 m_e^{1/2} m_h^{3/2} \right)^{1/2} \right] \quad (3)$$

$$\ln(T^2 \tau) \approx \left(\frac{\Delta E}{k_B T} \right) - \ln \left[\left(\frac{4k_B^2 \sigma_p}{gh^3} \right) \left(6\pi^3 m_e^{3/2} m_h^{1/2} \right)^{1/2} \right] \quad (4)$$

where ΔE is the trap-energy, σ_n , σ_p are the electron and hole capture cross sections, g is the degeneracy factor, and m_e , m_h are the electron and hole effective masses, respectively. For these relationships, it is assumed that the semiconductor is at or near thermal equilibrium, which is the case for low applied biases. Dependences of $\ln(T^2 \tau)$ versus $1/k_B T$ are shown in Fig. 8 for all the four types of NWs; a good agreement to the theory is seen for all FETs. From the slope of the plot in Fig. 8, we can extract the energy position of the trap-level and the intercept will give us the capture cross sections. Once energy level and capture cross sections are determined from the slope and the intercept of the curves in Fig. 8, the trap-concentration N_T can be estimated using the following simplified relationship $\tau \approx 1/(\sigma_e v_e N_T)$, where v_e is the thermal velocity of the electrons given by [28]

$$v_e = \sqrt{3k_B T/m_e}. \quad (5)$$

The estimated energy levels, electron and hole capture cross sections, and concentrations of the traps are listed in Table I. There are few key points worth mentioning about the estimates obtained using LFN spectroscopy: 1) unlike DLTS, LFN spectroscopy cannot determine specifically the position of the trap relative to the conduction or valence bands and 2) the degeneracy factors in (3) and (4) introduce uncertainty in the determination of the capture cross sections and trap density, as the degeneracy factors for transition metals in silicon can vary from fractional values to integers [29]–[31]. However, this error should be small compared with the magnitudes of capture cross sections and trap densities. We have assumed $g = 1$ for the calculations.

The most established data on the energy levels introduced by Ni and Au impurities in Si are listed in Table II after [32]. Comparing Tables I and II, we see a good agreement between our estimated values of the traps in SiNWs and the accepted literature data for Ni and Au impurities. The only exception is the estimated Au-acceptor level. Our results also agree with the recent report by Sato *et al.* [15] who detected two levels with activation energy of 0.36 and 0.38 eV in *p*-type and

n-type VLS grown Si NWs, respectively, and associated them with electrically active Au–H complexes. As for Ni-catalyzed SiNWs, we believe that this is the first report on detection of deep levels introduced by Ni in SiNWs. Data on capture cross sections of Ni traps in Si are limited. Capture cross sections in the range of $1\text{--}5 \times 10^{-16} \text{ cm}^{-2}$ were estimated for a Ni electron trap at ($E_c - 0.48 \text{ eV}$) in n-Si [33]. Using DLTS technique, Tavendale and Pearton [34] determined capture cross section in the range 10^{-20} cm^{-2} for a Ni hole trap at ($E_v + 0.33 \text{ eV}$) in p-type Si. This is in line with the capture-cross sections associated with Ni levels estimated in this paper. The electron and hole capture cross sections for the Au donor state were reported in the range $2\text{--}6 \times 10^{-15} \text{ cm}^{-2}$ [35]. By combining DLTS and PICTS, Sato *et al.* determined hole and electron capture cross sections of the Au–H complex (0.36 eV) to be $3 \times 10^{-18} \text{ cm}^{-2}$ and $1 \times 10^{-15} \text{ cm}^{-2}$, respectively.

Ni is a fast diffuser in Si with large fraction of Ni atoms occupying the interstitial sites. It has been established that only $\sim 0.1\%$ of dissolved Ni atoms occupy substitutional sites and are electrically active [36]. Istratov *et al.* [37] found that Ni solubility does not vary significantly for n-type and p-type silicon. For diffusion temperatures between $900 \text{ }^\circ\text{C}$ and $1000 \text{ }^\circ\text{C}$, the Ni concentration was in the range $7\text{--}20 \times 10^{16} \text{ cm}^{-3}$. Thus, expected concentration of substitutional Ni atoms, i.e., traps, would be in the range $10^{13}\text{--}10^{14} \text{ cm}^{-3}$. Our estimated trap concentration for Ni-catalyzed n-type is slightly lower than that range, however for p-type wires estimated trap concentration is approximately two orders higher. Our estimated Au-related trap concentration value is roughly three orders of magnitude lower than the equilibrium solubility of gold in silicon at $850 \text{ }^\circ\text{C}$ ($\approx 2 \times 10^{15} \text{ cm}^{-3}$) as calculated from the thermal diffusion data [38]. The lower trap density could be either due to the actual lower Au concentration in the SiNW matrix or due to the hydrogen passivation of Au traps [39].

IV. CONCLUSION

Four different sets of FETs were fabricated using Au- and Ni-catalyzed n- and p-doped SiNWs. Correlated noise measurement technique enabled us to perform accurate noise measurements on these low current nanoscale devices by effectively reducing the instrument noise. We identified deep-levels in these Ni and Au catalyzed n- and p-doped SiNWs, which matches very closely the known ionization energies of Ni and Au impurities in Si. To the best of our knowledge, this is the first report of deep-levels introduced by Ni-catalyst in SiNWs. In summary, our study demonstrates that optimized LFN measurement can be a powerful tool for studying electrically active defects in nanoscale devices, especially when conventional defect characterization techniques cannot be implemented.

REFERENCES

- [1] R. M. Y. Ng, W. Tao, and M. Chan, "A new approach to fabricate vertically stacked single-crystalline silicon nanowires," in *Proc. IEEE Conf. EDSSC*, Dec. 2007, pp. 133–136.
- [2] M. H. Ben Jamaa, K. E. Moselund, D. Atienza, D. Bouvet, A. M. Ionescu, Y. Leblebici, *et al.*, "Fault-tolerant multi-level logic decoder for nanoscale crossbar memory arrays," in *Proc. IEEE/ACM ICCAD*, Nov. 2007, pp. 765–772.
- [3] J. Fu, N. Singh, K. D. Buddharaju, S. H. G. Teo, C. Shen, Y. Jiang, *et al.*, "Si-nanowire based gate-all-around nonvolatile SONOS memory cell," *IEEE Electron Device Lett.*, vol. 29, no. 5, pp. 518–521, May 2008.
- [4] J. M. Larson and J. P. Snyder, "Overview and status of metal S/D Schottky-barrier MOSFET technology," *IEEE Trans. Electron Devices*, vol. 53, no. 5, pp. 1048–1058, May 2006.
- [5] J. Appenzeller, J. Knoch, M. T. Bjork, H. Riel, H. Schmid, and W. Riess, "Toward nanowire electronics," *IEEE Trans. Electron Devices*, vol. 55, no. 11, pp. 2827–2845, Nov. 2008.
- [6] S. A. Dayeh, "Electron transport in indium arsenide nanowires," *Semicond. Sci. Technol.*, vol. 25, no. 2, pp. 024004-1–024004-20, Feb. 2010.
- [7] A. Motayed, M. Vaudin, A. V. Davydov, J. Melngailis, M. He, and S. N. Mohammad, "Diameter dependent transport properties of gallium nitride nanowire field effect transistors," *Appl. Phys. Lett.*, vol. 90, no. 4, pp. 043104-1–043104-3, Jan. 2007.
- [8] J. Jie, W. Zhang, K. Peng, G. Yuan, C. S. Lee, and S.-T. Lee, "Surface-dominated transport properties of silicon nanowires," *Adv. Funct. Mater.*, vol. 18, no. 20, pp. 3251–3257, Oct. 2008.
- [9] J. E. Allen, E. R. Hemesath, D. E. Perea, J. L. Lensch-Falk, Z. Y. Li, F. Yin, *et al.*, "High-resolution detection of Au catalyst atoms in Si nanowires," *Nat. Nanotechnol.*, vol. 3, no. 3, pp. 168–173, Mar. 2008.
- [10] M. Bar-Sadan, J. Barthel, H. Shtrikman, and L. Houben, "Direct imaging of single Au atoms within GaAs nanowires," *Nano Lett.*, vol. 12, no. 5, pp. 2352–2356, Apr. 2012.
- [11] W. Shockley and W. T. Read, "Statistics of the recombinations of holes and electrons," *Phys. Rev.*, vol. 87, no. 5, pp. 835–842, Sep. 1952.
- [12] J. Goldberger, A. I. Hochbaum, R. Fan, and P. Yang, "Silicon vertically integrated nanowire field effect transistors," *Nano Lett.*, vol. 6, no. 5, pp. 973–977, Mar. 2006.
- [13] S. C. Rustagi, N. Singh, W. W. Fang, K. D. Buddharaju, S. R. Omampuliyur, S. H. G. Teo, *et al.*, "CMOS inverter based on gate-all-around silicon-nanowire MOSFETs fabricated using top-down approach," *IEEE Electron Device Lett.*, vol. 28, no. 11, pp. 1021–1024, Nov. 2007.
- [14] D. K. Schroder, *Semiconductor Material and Device Characterization*. New York, NY, USA: Wiley, 1990.
- [15] K. Sato, A. Castaldini, N. Fukata, and A. Cavallini, "Electronic level scheme in boron- and phosphorus-doped silicon nanowires," *Nano Lett.*, vol. 12, no. 6, pp. 3012–3017, Apr. 2012.
- [16] A. Motayed, S. Krylyuk, and A. V. Davydov, "Characterization of deep-levels in silicon nanowires by low-frequency noise spectroscopy," *Appl. Phys. Lett.*, vol. 99, no. 11, pp. 113107-1–113107-3, Sep. 2011.
- [17] M. Sampietro, L. Fasoli, and G. Ferrari, "Spectrum analyzer with noise reduction by cross-correlation technique on two channels," *Rev. Sci. Instrum.*, vol. 70, no. 5, pp. 2520–2525, Jan. 1999.
- [18] S. M. Sze and K. K. Ng, *Physics of Semiconductor Devices*, 3rd ed. New York, NY, USA: Wiley, 2007.
- [19] H. D. Xiong, W. Wang, Q. Li, C. A. Richter, J. S. Suehle, W.-K. Hong, *et al.*, "Random telegraph signals in n-type ZnO nanowire field effect transistors at low temperature," *Appl. Phys. Lett.*, vol. 91, no. 5, pp. 053107-1–053107-3, Jul. 2007.
- [20] A. Van der Ziel, *Fluctuation Phenomena in semi-conductor*. London: Butterworths Scientific Publications, 1959.
- [21] A. L. McWhorter, "1/f noise and related surface effects in germanium," Ph.D. dissertation, Dept. Elect. Eng., Massachusetts Institute Tech., Cambridge, MA, USA, 1955.
- [22] J. J. Brophy and R. J. Robinson, "Current noise due to ohmic contacts on cadmium sulfide," *J. App. Phys.*, vol. 31, no. 8, pp. 1343–1344, Jul. 1960.
- [23] P. T. Landsberg, C. Rhys-Roberts, and P. Lal, "Auger recombination and impact ionization involving traps in semiconductors," *Proc. Phys. Soc.*, vol. 84, no. 6, pp. 910–915, Dec. 1964.
- [24] C. T. Sah and L. D. Yau, "Observation of the ideal generation-recombination noise spectrum and spectra with voltage variable relaxation time in gold-doped silicon," *Appl. Phys. Lett.*, vol. 14, no. 9, pp. 267–269, May 1969.
- [25] C. T. Sah, "Theory of low-frequency generation noise in junction-gate field-effect transistors," *Proc. IEEE*, vol. 52, no. 7, pp. 795–814, Jul. 1964.
- [26] F. Scholz, J. M. Hwang, and D. K. Schroder, "Low frequency noise and DLTS as semiconductor device characterization tools," *Solid-State Electron.*, vol. 31, no. 2, pp. 205–217, Feb. 1988.

- [27] F. J. Scholz and J. W. Roach, "Low-frequency noise as a tool for characterization of near-band impurities in silicon," *Solid-State Electron.*, vol. 35, no. 4, pp. 447–452, Apr. 1992.
- [28] G. Bemski, "Recombination properties of gold in silicon," *Phys. Rev.*, vol. 111, no. 6, pp. 1515–1518, Sep. 1958.
- [29] W. M. Bullis and F. J. Strieter, "Electrical properties of N-type silicon doped with gold," *J. App. Phys.*, vol. 39, no. 1, pp. 314–318, Jan. 1968.
- [30] A. F. Tasch and C. T. Sah, "Recombination-generation and optical properties of gold acceptor in silicon," *Phys. Rev. B*, vol. 1, no. 2, pp. 800–809, Jan. 1970.
- [31] H. I. Ralph, "Degeneracy factor of gold acceptor level in silicon," *J. App. Phys.*, vol. 49, no. 2, pp. 672–675, 1978.
- [32] P. Siffert and E. F. Krimmel, *Silicon: Evolution and Future of a Technology*. New York, NY, USA: Springer-Verlag, 2004.
- [33] S. Sato, A. Memon, A. Fukuyama, S. Tanaka, and T. Ikari, "Deep level photothermal spectroscopy for characterizing Ni impurities in Si by a temperature dependent piezoelectric photothermal signal," *Rev. Sci. Instrum.*, vol. 74, no. 1, pp. 340–342, Jan. 2003.
- [34] A. J. Tavendale and S. J. Pearton, "Deep level, quenched-in defects in silicon doped with gold, silver, iron, copper or nickel," *J. Phys. C, Solid State Phys.*, vol. 16, no. 9, pp. 1665–1673, Oct. 1983.
- [35] A. G. Milnes, *Deep Impurities in Semiconductors*. New York, NY, USA: Wiley, 1973.
- [36] S. Tanaka, T. Ikari, and H. Kitagawa, "In-diffusion and annealing processes of substitutional nickel atoms in dislocation-free silicon," *Jpn. J. Appl. Phys.*, vol. 40, no. 5A, pp. 3063–3068, May 2001.
- [37] A. A. Istratov, P. Zhang, R. J. McDonald, A. R. Smith, M. Seacrist, J. Moreland, *et al.*, "Nickel solubility in intrinsic and doped silicon," *J. App. Phys.*, vol. 97, no. 2, pp. 023505-1–023505-6, Jan. 2005.
- [38] N. A. Stolwijk, B. Schuster, and J. Hölzl, "Diffusion of gold in silicon studied by means of neutron-activation analysis and spreading-resistance measurements," *Appl. Phys. A*, vol. 33, no. 2, pp. 133–140, Feb. 1984.
- [39] S. J. Pearton and A. J. Tavendale, "Hydrogen passivation of gold-related deep levels in silicon," *Phys. Rev. B*, vol. 26, no. 12, pp. 7105–7108, Dec. 1982.



Deepak Sharma is currently pursuing the Ph.D. degree with George Mason University, Fairfax, VA, USA.

He has been a Guest Researcher with the Material Measurement Laboratory, NIST, since 2011.



Abhishek Motayed received the Ph.D. degree from the Electrical and Computer Engineering Department, University of Maryland, College Park, MD, USA, in 2007.

He is a Research Scientist with the Institute of Research in Electronics and Applied Physics, University of Maryland.



Sergiy Krylyuk received the Ph.D. degree in physics of semiconductors from Chernivtsi National University, Chernivtsi, Ukraine, in 1999.

He has been with the Institute of Research in Electronics and Applied Physics, University of Maryland, College Park, MD, USA, since 2010.



Qiliang Li (M'04) received the Ph.D. degree in electrical and computer engineering from North Carolina State University, Raleigh, NC, USA, in 2004.

He joined the faculty of the Department of Electrical and Computer Engineering, George Mason University, Fairfax, VA, USA, in 2007.



Albert V. Davydov received the Ph.D. degree in chemistry from Moscow State University, Moscow, Russia, in 1989.

He is currently a Leader of the Functional Nanostructured Materials Group, Materials Science and Engineering Division, Material Measurement Laboratory, NIST.